Article:
Hubbard, CH, West, LJ, Morris, K et al. (4 more authors) (2011) In search of experimental evidence for the biogeobattery. Journal of Geophysical Research Biogeosciences, 116. ISSN 2169-8996

https://doi.org/10.1029/2011JG001713

In search of experimental evidence for the biogeobattery

Christopher G. Hubbard,[1] L. Jared West,[1] Katherine Morris,[2] Bernd Kulessa,[3] Diana Brookshaw,[2] Jonathan R. Lloyd,[2] and Samuel Shaw[1]

Received 22 March 2011; revised 15 August 2011; accepted 17 August 2011; published 15 November 2011.

[1] Recent work has suggested that the electrical self-potential (SP) geophysical technique may be used to noninvasively map redox conditions associated with contaminant plumes or bioremediation schemes. The proposed mechanism linking SP response and redox involves the generation of a current source and sink in the subsurface whereby electrons are transferred between anoxic and oxic environments via a conductive biofilm and/or biominerals, creating a biogeobattery. To investigate the conditions required for biogeobattery formation, we successfully created contrasting redox zones in a flow-through column setup. In this setup, an oxic section, containing clean sand, transitioned into an Fe(III)-reducing section. Fe(III) reduction was mediated by either a natural microbial community or a pure culture of the model organism *Shewanella oneidensis* MR-1 in two different column experiments. Visual observations and electron microscopy showed that ferrihydrite was sequentially transformed to goethite and magnetite; despite this change, no SP signal was generated in either column. Electron microscopy suggested that in the pure culture column, *S. oneidensis* MR-1 cells did not form a continuous, interconnected biofilm but rather interacted with the iron (oxyhydr)oxide surfaces as individual cells. In our experiments we therefore did not form the conductor of the biogeobattery. We thus conclude that generation of a biogeobattery is nontrivial and requires specific geochemical and microbiological conditions that will not occur at every contaminated site undergoing microbially mediated redox processes. This conclusion suggests that SP cannot be used in isolation to monitor subsurface biogeochemical conditions.

Citation: Hubbard, C. G., L. J. West, K. Morris, B. Kulessa, D. Brookshaw, J. R. Lloyd, and S. Shaw (2011), In search of experimental evidence for the biogeobattery, *J. Geophys. Res.*, *116*, G04018, doi:10.1029/2011JG001713.

1. Introduction

[2] The rapidly evolving field of biogeophysics seeks to link geophysical signatures with microbially induced changes in the subsurface [*Atekwana and Slater*, 2009]. One of the principal goals of this discipline is to develop a suite of noninvasive techniques that can be used from the ground surface. Such techniques are vitally important in tracking the progress of contaminant plumes (e.g., hydrocarbons and metals, including radionuclides) and in situ remediation schemes (e.g., biostimulation) [*Anderson et al.*, 2003; *Williams et al.*, 2009]. Compared with conventional borehole sampling and laboratory analysis, biogeophysical techniques may thus prove to be a low-cost approach with greatly enhanced spatiotemporal resolution. This approach is particularly relevant to some nuclear legacy sites, such as areas of Hanford and Oak Ridge in the United States and Sellafield in the United Kingdom [*Hunter*, 2004; *Catalano et al.*, 2006; *Kelly et al.*, 2008], where noninvasive surveys may be the only practicable option for assessing the state of the subsurface because of the potentially very high radiotoxicity of contaminant plumes. Even in scenarios where radioactivity is present at relatively low levels (e.g., uranium mining or low level waste disposal sites such as Drigg in the United Kingdom [*Wilkins et al.*, 2007]), noninvasive approaches offer potentially massive improvements as they avoid compromising the integrity of the subsurface hydrogeochemistry. One of the most promising noninvasive techniques is electrical self-potential (SP), which is a passive geophysical technique capable of sensing naturally generated currents in the subsurface. SP is of particular interest in biogeophysics as a potential noninvasive sensor of redox conditions in subsurface sediments [*Jouniaux et al.*, 2009; *Revil et al.*, 2010]. This use is important as microbially induced reducing conditions (e.g., iron reducing or sulfate reducing) often limit contaminant mobility in the environment by influencing chemical speciation of radioactive contaminants (e.g., reducing U(VI), Np(V), and Tc(VII) to poorly soluble U(IV), Np(IV), and Tc(IV) [*Law et al.*, 2010a, 2010b; *Lear et al.*, 2010; *Begg et al.*, 2011]) or by creating favorable conditions for microbial degradation of

[1]Earth Surface Science Institute, School of Earth and Environment, University of Leeds, Leeds, UK.
[2]Research Centre for Radwaste and Decommissioning and Williamson Centre for Molecular Environmental Science, School of Earth, Atmospheric and Environmental Sciences, University of Manchester, Manchester, UK.
[3]School of the Environment and Society, University of Swansea, Swansea, UK.

0148-0227/11/2011JG001713

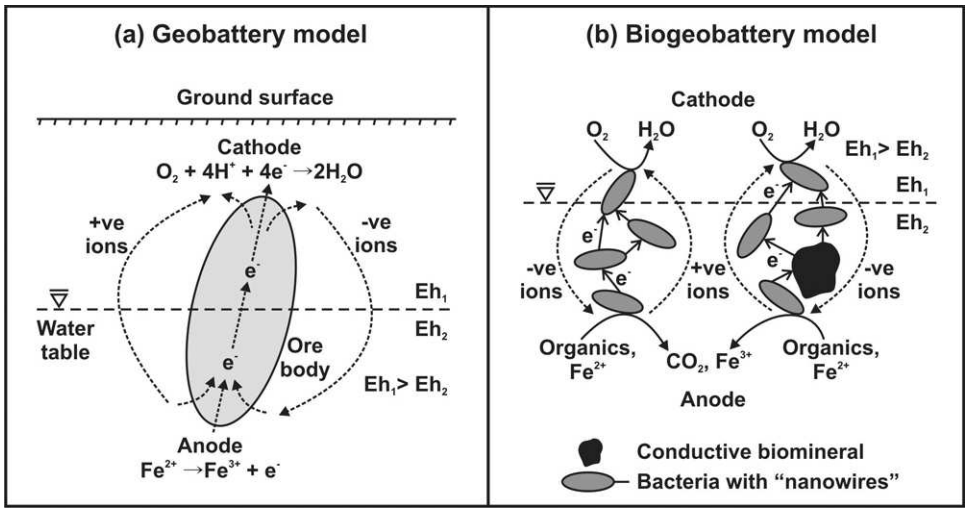

Figure 1. Conceptual models of redox-associated mechanisms for generating self-potentials: (a) classical geobattery model [after *Sato and Mooney*, 1960; *Revil et al.*, 2010] and (b) biogeobattery model [after *Naudet and Revil*, 2005; *Revil et al.*, 2010].

organic contaminants (e.g., reductive dechlorination of trichloroethene [*Fennell et al*., 2001]).

[3] SP measures the electrical potential distribution resulting from a current source in the subsurface. This current source may be generated from groundwater flow (streaming potentials) or variations in the concentration and distribution of charged ions (electrochemical diffusion potentials) [*Reynolds*, 1997]. Large SP signatures (>100 mV) can also be generated by a geobattery formed when an electronic conductor links geochemically distinct redox environments [*Reynolds*, 1997; *Jouniaux et al.*, 2009]. In the classical geobattery model (Figure 1a), the conductor is an ore body straddling the water table [*Sato and Mooney*, 1960], with charge being transferred between electronic and ionic charge carriers by the redox half-reactions occurring in the vadose and saturated zones. The return current pathway is via ionic charge carriers in the pore fluid surrounding the ore body. Redox-associated SP anomalies have also been described at field sites contaminated by landfill leachate and chlorinated organic solvents [*Naudet et al.*, 2004; *Arora et al.*, 2007; *Minsley et al.*, 2007]. The suggested mechanism is a "biogeobattery" (Figure 1b), where the conductor is a bacterial biofilm and/or conductive biominerals (e.g., magnetite, Fe_3O_4) straddling a redox gradient (e.g., the water table or the plume fringe), with the return current pathway through the surrounding pore fluid. However, no direct experimental evidence has been produced to validate the biogeobattery hypothesis and determine the mechanism of SP anomaly formation associated with contaminant plumes.

[4] In this study we sought to refine our understanding of the key components needed to form a biogeobattery. We used a combined geophysical and biogeochemical laboratory-based approach specifically designed for this purpose where geophysical, geochemical, mineralogical, and biological parameters were characterized on the same system. We utilized a flow-through column system containing either a natural microbial community present within sediment or a cultured Fe(III)-reducing microorganism (*Shewanella oneidensis* MR-1) to promote Fe(III)-reducing conditions, and thus we create a redox gradient within a bioavailable ferrihydrite coated quartz sand column. SP was monitored with nonpolarizing electrodes, the geochemistry of the pore fluid was analyzed using electrochemical measurements (i.e., Eh) and biogeochemical indicators (e.g., dissolved Fe(II) concentration), and high-resolution electron microscopy was used to characterize the development of the conductors proposed in the biogeobattery model (i.e., bacterial biofilm or conductive biominerals).

2. Materials and Methods

2.1. Overview

[5] Two column experiments were performed; the setup used for both is shown in Figure 2. In both experiments, pure quartz sand coated with 2-line ferrihydrite was used as a bioavailable Fe(III) substrate [*Hansel et al.*, 2003]. The use of a pure mineral phase rather than a natural substrate made it simpler to investigate mineral transformations that occurred as a result of microbial Fe(III) reduction. Column 1 used a matrix commonly employed in biogeophysics experiments (Ottawa sand, Fisher Scientific; 590–840 μm in diameter; [*Ntarlagiannis et al.*, 2005; *Williams et al.*, 2007]) and was inoculated with natural sediment representative of the Sellafield nuclear site in the United Kingdom to represent real-world conditions. Microbial reduction of Fe(III) was stimulated by addition of growth medium at a relatively low flow rate (~0.25 pore volumes per day) to allow sufficient residence time in the column for the natural microbial consortia to reduce the initially oxic influent waters. The column 1 experiment ran for 131 days. Following the completion of column 1, column 2 was designed to optimize Fe(III) reduction and the formation of conductive biominerals (in this case, magnetite Fe_3O_4) by using a pure culture of a model Fe(III)-reducing organism, *Shewanella oneidensis* MR-1. Here, the experimental design closely followed the procedure of *Hansel et al.* [2003], except that a finer quartz sand (Iota-6, Unimin Corporation, Connecticut; 105–297 μm) was used to give a higher surface area and hence a greater concentration of bio-

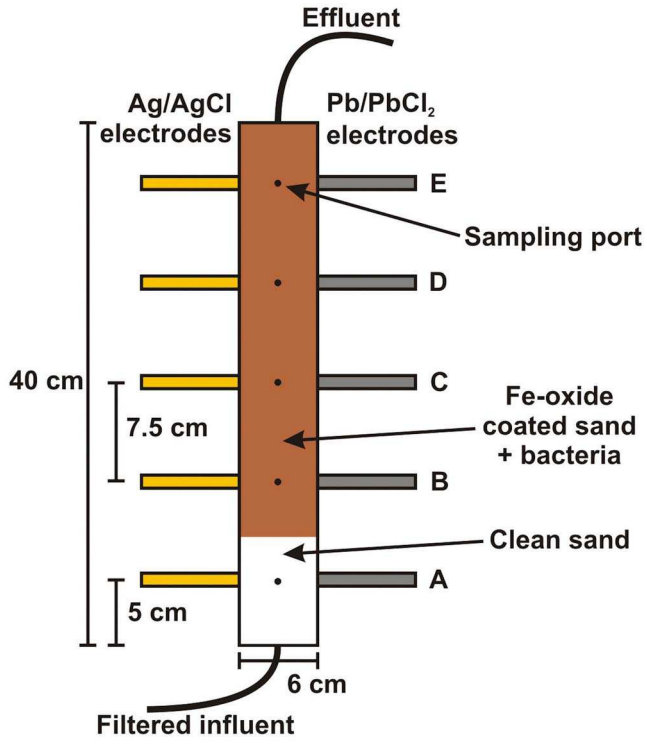

Figure 2. Experimental setup. Sample ports/electrodes labeled A–E from bottom.

available Fe(III) in the column. Note that no natural sediment was added to column 2. A higher flow rate of ~0.75 pore volumes per day was chosen because faster Fe(III) reduction was expected in this optimized system [*Hansel et al.*, 2003], and the experiment ran for 43 days.

2.2. Porous Media

[6] Quartz sands were coated with 2-line ferrihydrite using the methods described by *Brooks et al.* [1996] and *Hansel et al.* [2003]. Briefly, 2-line ferrihydrite was precipitated by rapidly titrating 0.062 *M* ferric chloride solution with 0.4 *M* NaOH to pH 7.5. After the mineral phase was washed with deionized water to remove salts, the ferrihydrite suspension was mixed with pure quartz sand and dried at room temperature, with repeated stirring to ensure uniform coating of the sand. Ferrihydrite mineralogy was confirmed with powder X-ray diffraction (XRD) using a Philips PW1050 diffractometer. The final Fe concentration was determined by digesting 1 g of sand in 5 mL of 6 *M* HCl for 8 h [*Hansel et al.*, 2003] and analyzing Fe using the ferrozine assay [*Stookey*, 1970]. Porosity was calculated by dry-packing a column, filling it with water from the base at a known rate using a high-performance liquid chromatography (HPLC) pump and measuring the time taken until full saturation. This yielded porosities of 0.37 for the Ottawa sand and 0.42 for the Iota-6 sand. Before loading the sand into the columns, it was sterilised by autoclaving at 121°C for 15 min in the media solution used for each experiment.

2.3. Bacteria and Growth Media

[7] Column 1 was inoculated with a natural microbial consortium capable of Fe(III) reduction by mixing ferrihydrite-coated sand with ~5% by volume of a natural silty-sandy sediment representative of the Quaternary unconsolidated alluvial floodplain deposits that underlie the Sellafield nuclear facility [*Law et al.*, 2010a]. In natural sediments, much of the Fe can be in minerals that are relatively recalcitrant to microbial metabolism, such as silicates. The bioavailable Fe(III) was therefore estimated by digesting 0.1 g of sediment in 0.5 *M* HCl [*Lovley and Phillips*, 1987]. The flow-through medium used in the column experiment had a fluid conductivity of ~1.4 mS/cm and was based on a representative regional synthetic groundwater media [*Wilkins et al.*, 2007; *Law et al.*, 2010a] (89 μM KCl, 398 μM $MgCl_2$, 161 μM NaCl, 0.5 m*M* NaBr, 680 μM Na_2SiO_3, 18 μM NH_4Cl, 7 μM KH_2PO_4), buffered at pH 7.5 with 10 m*M* MOPS (3-morpholinopropane-1-sulfonic acid). Sodium acetate (10 m*M*) was added as an electron donor. No nitrate or sulfate was added to the media to ensure that O_2(aq) and Fe(III) were the dominant terminal electron acceptors in the system, as the natural microbial consortium is capable of metabolizing a wide range of electron acceptors [*Law et al.*, 2010a].

[8] Column 2 was inoculated with *S. oneidensis* MR-1, which was grown aerobically to late log phase at room temperature in *Shewanella* minimal medium solution [*von Canstein et al.*, 2008]. Cells were harvested by centrifugation, washed twice, and resuspended in 10 m*M* MOPS buffer (pH 7.5). The flow-through medium used had a fluid conductivity of ~1.7 mS/cm and was modified from *Hansel et al.* [2003] (67 μM KCl, 415 μM $MgSO_4$, 513 μM NaCl, 0.5 m*M* NaBr, 18 μM NH_4Cl, 7 μM KH_2PO_4, and 1 mL/L trace minerals solution), buffered to pH ~7.2 with 10 m*M* PIPES (1,4-piperazinediethanesulfonic acid). Sodium lactate (3 m*M*) was used as the electron donor. *S. oneidensis* MR-1 was added to the autoclaved sand (presaturated with media) before the sand was packed into the column; the microbial concentration was ~10^8 cells/mL. The cells were rested (for 4.5 h) to allow them to adhere to the sand matrix before the flow experiment began [*Hansel et al.*, 2003].

2.4. Column Setup

[9] Experiments were conducted in acrylic columns with 6 cm internal diameter and 40 cm length (Figure 2). Electrodes for SP measurements and solution sampling points were located at 5.0, 12.5, 20.0, 27.5, and 35.0 cm from the column base. Column and tubing materials were presterilized prior to being packed with sand. The bottom section of the column (8.8 cm, column 1; 9.5 cm, column 2) was packed with uncoated, clean, sterile sand to establish an oxic section within the column. The rest of the column contained inoculated, ferrihydrite-coated sand to create a contrasting Fe-reducing section. Flow-through growth medium (see section 2.3) was pumped into the bottom of each column through a 0.2 μm filter using a LabAlliance Series II isocratic HPLC pump, and the influent medium was bubbled through with 0.2 μm filter sterilized air to ensure that it remained oxygenated. Column 1 was preequilibrated with 10 pore volumes of media before the experiment was started to allow the pH to buffer to circumneutral. Flow velocities were maintained at 0.1 m/d (pump rate of 0.07 mL/min) for column 1 and 0.3 m/d (0.25 mL/min) for column 2.

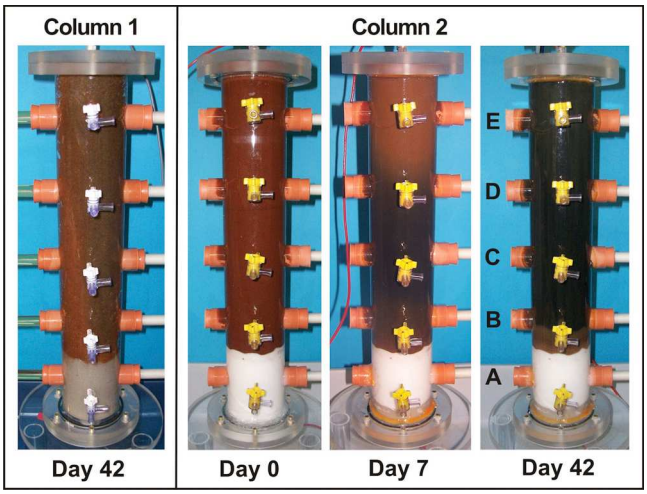

Figure 3. Visual observations of (left) column 1 at day 42 and (right) column 2 at day 0, 7 and 42. Sample ports/electrodes labeled A–E from bottom.

2.5. Self-Potential Measurements

[10] Previous studies have shown that electrode selection is extremely important in biogeophysics laboratory experiments; Ag/AgCl electrodes are a common choice of nonpolarizing electrode but can react with dissolved sulfide to create galvanic cell potentials that are not reflective of SP [*Williams et al.*, 2007; *Slater et al.*, 2008; *Zhang et al.*, 2010]. We reduced the likelihood of galvanic cell potentials by using SP electrodes in a gel or clay matrix isolated from the column fluid chemistry and by optimizing conditions for Fe(III) reduction rather than sulfate reduction.

[11] In the column 1 experiment, we directly compared the performance of two sets of nonpolarizing electrodes for use in SP measurements. Miniaturized $Pb/PbCl_2$ electrodes [*Petiau*, 2000] were installed on one side of the column at 5.0, 12.5, 20.0, 27.5, and 35.0 cm from the column base (Figure 2). The custom-built electrodes consisted of Pb wire coils inside acrylic tubes containing kaolin clay saturated with NaCl and $PbCl_2$ and closed with porous wood end caps; the dimensions of the electrodes were designed to ensure saturation was maintained for ~14 months. Commercial Ag/AgCl electrodes (Sensorex Corporation, California) in a KCl gel were installed on the opposite side of the column (Figure 2). SP measurements were logged every 15 min using Campbell Scientific CR10X loggers (input resistance ~20 GΩ). The reference electrode was the bottom SP electrode for each set, which was located in the clean sand section of the column, which was receiving oxic influent medium. On the basis of the evaluation of electrode performance in column 1 (see section 3.4), only $Pb/PbCl_2$ electrodes were used in column 2.

2.6. Geochemical and Mineralogical Sampling and Measurements

[12] Fluid samples were obtained from the influent and column sampling ports. Syringes and sampling ports were flushed with nitrogen prior to sampling to minimize sample oxidation. Samples were filtered (<0.2 μm) and analyzed for Eh, pH, and fluid conductivity. Dissolved Fe(II) was determined using the ferrozine assay [*Stookey*, 1970], while chloride was determined by ion chromatography using a Dionex DX600. At the end of the experiments, solid samples were carefully removed from the columns and prepared for scanning electron microscope (SEM) characterization by fixing the bacterial cells in 2.5% gluteraldehyde solution, washing with a 0.1 *M* phosphate buffer, dehydrating in a graded acetone series, critical point drying, and coating with platinum [*Vandevivere and Baveye*, 1992]. Characterization was done on an FEI Quanta 200F FEG-ESEM in secondary electron mode.

3. Results

3.1. Characterization of Ferrihydrite-Coated Sand and Initial Sediment

[13] XRD confirmed that the synthesized iron oxyhydroxide was 2-line ferrihydrite and that autoclaving this mineral in growth medium for 15 min at 121°C did not change the mineralogy. The Fe concentration of the ferrihydrite-coated sand was 8.6 ± 0.3 μM/g (mean ± 1σ, n = 5) for column 1 sand (590–840 μm in diameter) and 218 ± 16 μM/g (mean ± 1σ, n = 5) for the finer column 2 sand (105–297 μm in diameter). This 25 fold difference in Fe concentration was also reflected in the density of the ferrihydrite coating, with the fine column 2 sand having a more continuous coating, compared with isolated patches of ferrihydrite on the coarser column 1 sand (see auxiliary material Figures S1a and S1b).[1] The concentration of bioavailable Fe(III) in the natural sediment used as the microbial inoculum for column 1 was 6.0 ± 0.2 μM/g (mean ± 1σ, n = 4), similar to the concentration of Fe(III) for column 1 ferrihydrite-coated sand.

3.2. Visual and SEM Observations

[14] Column 1 had changed in color from orange to brown by day 35, although the color change was not uniform (see Figure 3a: column 1, day 42). The most dramatic visual changes were observed in column 2 (Figure 3b). The ferrihydrite-coated sand was initially orange-red, but by day 7, distinct zones were observed, with a dark brown-black section between sampling ports B and D contrasting strongly with an orange-brown section above port D. By day 14 (image not shown), this orange-brown section had also darkened to brown-black, and by the end of the experiment, the column was black in color from port B to the top of the column, with a small brown section in the ferrihydrite-coated sand below port B (Figure 3, day 42). The color changes seen in the columns matched those observed by *Hansel et al.* [2003] and are thus consistent with changes in iron mineralogy from orange-red ferrihydrite at the start of the experiment to brown goethite and then to black magnetite. Mineral transformation mechanisms are discussed later in section 4.2.

[15] SEM images from postexperimental analyses were used to provide further evidence of changes in iron mineralogy and to look for evidence of biofilm formation, as biofilms have been suggested to be the conductive component in the biogeobattery mechanism (Figure 1b and

[1] Auxiliary materials are available in the HTML. doi:10.1029/2011JG001713.

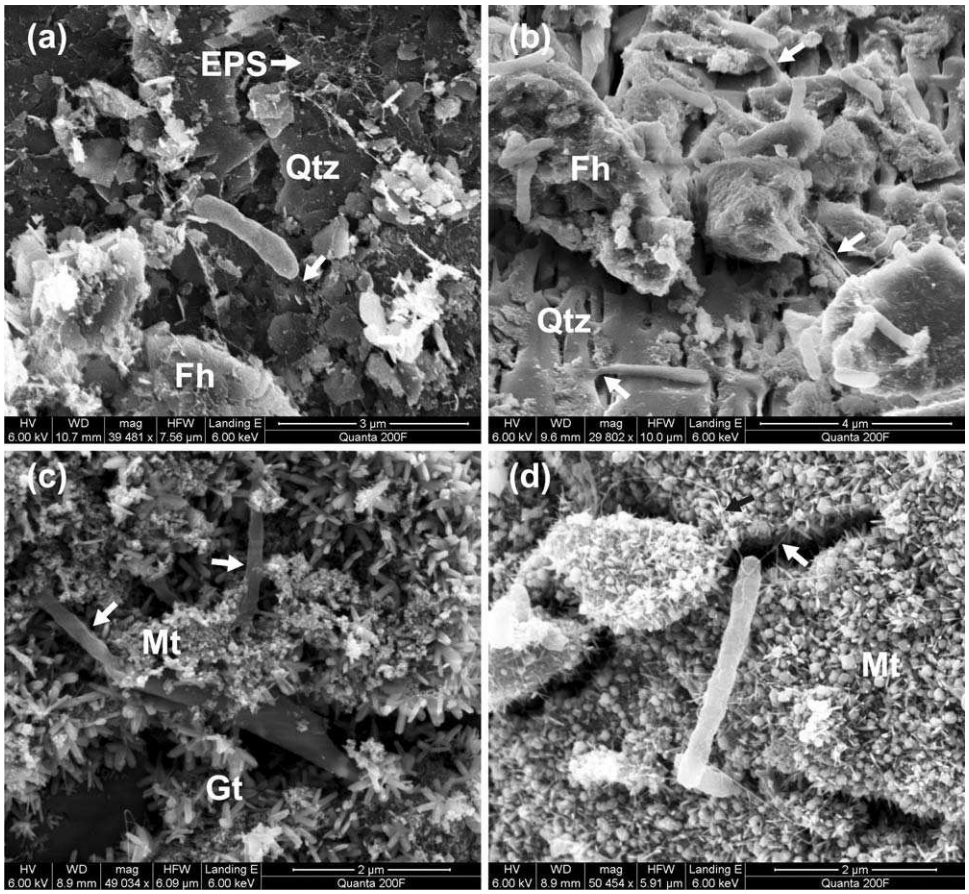

Figure 4. Scanning electron microscopy images of column media: column 1 (Figure 4a) and column 2 (Figures 4b–4d). (a) Single bacterium (center) and ferrihydrite on quartz. (b) *S. oneidensis* MR-1 cells on amorphous ferrihydrite (Fh) and on quartz (Qtz) surfaces; note that individual ferrihydrite particles cannot be resolved. (c and d) Single cells on variable amounts of acicular goethite (Gt) and cubic magnetite (Mt). Arrows on images indicate the position of extracellular polymer substances (EPS) and of filaments linking cells with iron oxides.

Revil et al. [2010]). Minerals were identified on the basis of crystal morphology and by comparison with column experiments using the same initial mineralogy and medium by *Hansel et al.* [2003], who confirmed their mineralogy using X-ray absorption fine structure spectroscopy (EXAFS). Column 1 was inoculated with natural sediment (~5% by volume) containing indigenous bacteria, mixed in with the ferrihydrite-coated sand. Some evidence for formation of extracellular polymer substances (EPS) was found (Figure 4a), but this evidence was not continuous over the surfaces of the sand grains. Goethite (α-FeOOH) needles were identified throughout column 1 (Figure S1c) and were typically associated with nanoparticulate ferrihydrite. Goethite formation is consistent with the color change seen in column 1 from orange to brown (Figure 3 and *Hansel et al.* [2003]).

[16] The ferrihydrite-coated sand in column 2 was inoculated with *S. oneidensis* MR-1 cells at high concentration (~10^8 cells/mL), and postexperimental SEM images show ~2 μm microbes distributed abundantly over the iron (oxyhydr)oxide-coated sand grains (Figure 4b). Cells appeared to be isolated from each other rather than forming an interconnected, continuous biofilm (Figure 4b). Filaments of varying thickness connecting bacterial cells to iron (oxyhydr)oxide mineral phases were occasionally observed (Figures 4b–4d) but did not interconnect cells to each other. The iron (oxyhydr)oxide mineral phase present in the first 2.5 cm of coated sand remained mainly as large, poorly ordered aggregates typical of the ferrihydrite coating the sand surface (Figure 4b), with acicular needles (15 × 100 nm), typical of goethite, visible only at higher magnification. The black section of column 2 contained variable amounts of goethite needles, together with 30–80 nm crystals displaying both cubic and octahedral morphology. These crystals were identified as magnetite on the basis of crystal morphologies (Figures 4c and 4d) and comparison with the results of *Hansel et al.* [2003].

3.3. Fluid Geochemistry

[17] The spatial and temporal variations in dissolved Fe(II) and Eh for both columns are summarized in Figure 5. Note that pH was buffered effectively by organic buffers (MOPS in column 1 and PIPES in column 2), maintaining values of

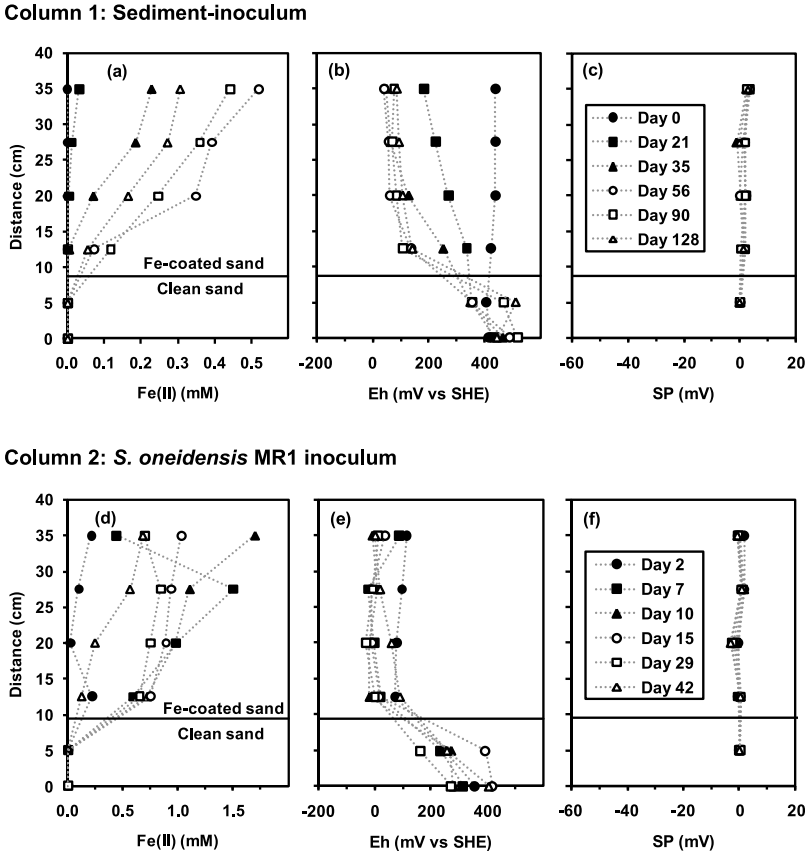

Figure 5. Spatiotemporal variation of (a, d) dissolved Fe(II), (b, e) Eh, and (c, f) SP for column 1 (Figures 5a–5c) and column 2 (Figures 5d–5f). Note the difference in scale (×10) for Eh and SP plots.

7.4–7.7 for column 1 and 6.8–7.3 for column 2 (data not shown). Microbial reduction of ferrihydrite released Fe(II) into solution and lowered the Eh in both columns. In column 1, Fe(III) reduction was relatively slow to develop as the acetate amendment stimulated the microbial population present in the added sediment, initially reducing the oxygen dissolved in the oxygen-saturated influent solution before Fe(III) reduction could occur. By day 21, low concentrations of dissolved Fe(II) (0.04 m*M*) were detected at port E, furthest (35 cm) from the column base; subsequently, more Fe(II) was progressively released into solution. The Eh profile evolved from a flat, oxic profile on day 0 (+407 to +438 mV versus standard hydrogen electrode) to a profile showing a steady decrease in Eh up the column on day 21 (+436 mV in the influent solution at 0 cm, Figure 5b, decreasing to +182 mV at 35 cm from the base) as Fe(III) reduction developed. By day 56, a marked contrast in Eh existed between the clean sand section of the column (+358 mV at 5 cm from the column base) and the iron (oxyhydr)oxide coated sand section (+138 mV at 12.5 cm from the column base, decreasing to +40 mV at 35 cm). Note that the decrease in Eh through the column (Figure 5b) is mirrored by increasing dissolved Fe(II) concentrations (Figure 5a, day 56: 0.07 m*M* at 12.5 cm increasing to 0.52 m*M* at 35 cm). After peaking at these values on day 56, Fe(II) concentrations then fell slowly (Fe(II) = 0.31 m*M*, Eh = +86 mV on day 128 at 35 cm from column base). Given the high flow rate of ~0.75 pore volumes per day, it is inferred that Fe(III) reduction was still occurring at the end of the experiment.

[18] In contrast to the natural sediment experiment, the high initial population of *S. oneidensis* MR-1 in column 2 resulted in rapid bioreduction within the first two days of the experiment. Dissolved Fe(II) concentrations generally increased up through column 2, were higher than in column 1 (up to 1.7 m*M* on day 10 at 35 cm from the column base), and peaked sooner (day 7 to 10), reflecting the high concentrations of microbial inoculate and the ~25 times higher solid (bioavailable) Fe(III) concentrations in this optimized system. Eh values were also lower than in column 1, reaching a minimum of −33 mV on day 29 at 20 cm from the column base. A clear Eh zonation was observed, with high Eh values in the influent solution (+356 ± 62 mV, mean ± 1σ, n = 11) and clean sand section (+274 ± 71 mV, mean ± 1σ, n = 11) contrasting with lower values in the iron (oxyhydr)oxide coated sand section (+14 ± 40 mV, mean ± 1σ, n = 44). The Eh measurements of solutions taken from the influent and the clean sand section in both columns showed high variability (Figures 5b and 5e), primarily reflecting the lack of electroactivity of O_2 at the platinum (Eh) electrode [*Stumm and Morgan*, 1981]. Nonetheless, a clear Eh contrast can be seen between the clean sand and Fe(III)-reducing zones of the column.

3.4. Self-Potential

[19] Previous studies have shown that Ag/AgCl electrodes in direct contact with pore waters can react with dissolved constituents (e.g., sulfide), leading to galvanic cell potentials that obscure the SP signals [*Williams et al.*, 2007; *Slater et al.*, 2008; *Zhang et al.*, 2010]. Column 1 directly compared the performance of two types of nonpolarizing electrodes where the metal electrode surface is isolated from the pore fluid to avoid galvanic cell potentials. In this experiment, $Pb/PbCl_2$ electrodes [*Petiau*, 2000], gave a more stable response than commercial Ag/AgCl electrodes in a KCl gel, which showed sensitivity to laboratory temperature variations (~3 mV/°C; see Figure S2 in the auxiliary material). The $Pb/PbCl_2$ electrodes consisted of a Pb wire in a clay matrix with a saturated solution of $PbCl_2$ and NaCl [*Petiau*, 2000]. A disadvantage of this electrode arrangement is that dissolved chloride concentrations increased up the column (e.g., from 1.4 m*M* to 3.6 m*M* on day 109), as a result of chloride diffusing out of the $Pb/PbCl_2$ electrodes, a result that again highlights the importance of electrode design in biogeophysics experiments.

[20] SP results are shown in Figure 5c and Figure 5f for the $Pb/PbCl_2$ electrodes in column 1 and column 2, respectively. According to the (bio)geobattery theory [*Revil et al.*, 2010], assuming that a conductor (e.g., a conductive biofilm or mineral phase, or both) is present in the column to transfer electrons across the redox transition, the SP measured relative to the reference electrode at the base of the column should be the opposite polarity to the change in Eh (i.e., positive) and reach a maximum magnitude equal to the change in Eh. This reasoning would give maximum SP responses of approximately +220 mV for column 1 (based on the Eh measurements on day 56 at 5 cm, in clean sand, and at 12.5 cm, in iron (oxyhydr)oxide coated sand) and +260 mV for column 2 (based on the measured mean Eh in the clean and iron (oxyhydr)oxide coated sand sections). Any measured response would be smaller due to potential losses between the conductor and the electron donors/acceptors [*Revil et al.*, 2010]. However, the SP measured in columns 1 and 2 remained within ±5 mV of the reference electrode throughout the experiments: No biogeobattery was detected in the columns, despite clear redox zonation in both experiments.

[21] No evidence was found for strong electrokinetic or diffusion potentials (Figure 5). The difference in SP between flowing (0.1–0.3 m/d) and static pore fluid conditions was <0.5 mV. The generation of electrokinetic potentials requires zeta potentials to be significant, and this was not the case in our experiments, as the pH in both of the columns (6.8–7.7) was within the range of published values for the points of zero charge reported for the iron (oxyhydr)oxide minerals present (pH 6.3–9.5 [*Cornell and Schwertmann*, 2003]). The absence of strong SP anomalies arising from diffusion potentials (e.g., associated with the concentration gradient in Fe(II)) is likely to reflect the relatively uniform ionic strength of the pore fluid within the column (e.g., between 1.7 and 2.0 mS/cm on day 10, column 2). This value is substantially different from those found in the experiment of *Maineult et al.* [2006], who recorded an SP magnitude of up to 9 mV due to an advecting front of ~1.2 m*M* $FeCl_2$ (~0.3 mS/cm) into a sand body saturated with deionized water (0.034 mS/cm). Although the Fe(II) concentration gradient in our study is similar to that measured by *Maineult et al.* [2006], in our system the Fe(II) carries a much smaller proportion of ionic charge, resulting in only minor diffusion potentials.

4. Discussion

[22] No SP signals diagnostic of a geobattery were observed in this study, despite the robust development of Fe(III)-reducing conditions in these systems. In this section we explore the reasons for this observation and their wider implications using the framework of the biogeobattery model (Figure 1b). Fe(III) reduction occurred in both column experiments, successfully creating contrasting redox zones between the clean and iron (oxyhydr)oxide coated sand sections. However, a biogeobattery also needs a conductor linking the two redox zones, and this connector may not have developed in our experiments. The biogeobattery model proposes that this conductor is either (1) a microbial biofilm and/or (2) conductive (bio)minerals We discuss these conductive pathways further in the following sections. Finally, we discuss the nature of the return current pathway in our experiments and the wider implications of this study.

4.1. Microbial Fe(III) Reduction and Biofilm Formation

[23] The role of microbial biofilms as conduits for electron transfer between different redox zones was first suggested as a mechanism for SP generation by *Naudet et al.* [2004], on the basis of a strong correlation between Eh and SP over a landfill leachate plume. *Naudet and Revil* [2005] further showed in a sandbox experiment that a −50 mV SP anomaly developed progressively over a period of 45 h after an aliquot of natural sediment that had developed sulfate-reducing conditions was inserted into the oxic sand, although they were not able to establish the mechanism of conduction (e.g., biofilm or biomineral formation).The biogeobattery concept has been strengthened by research suggesting that the Fe(III)-reducing bacteria *Geobacter sulfurreducens* and *Shewanella oneidensis* may produce electrically conductive appendages or "nanowires" to transfer electrons to iron (oxyhydr)oxide surfaces [*Reguera et al.*, 2005; *Gorby et al.*, 2006]. Recently, *El-Naggar et al.* [2010] proved that nanowires produced by *S. oneidensis* MR-1 (the bacterial strain used in column 2 of this study) could conduct electricity, as they had directly measured electron transport rates along the lengths of the nanowires. Work on microbial fuels cells has also shown that interconnection between cells may aid electron transfer in biofilms where the outermost cells of the biofilm have no direct contact with the solid Fe(III) substrate [*Reguera et al.*, 2006].

[24] *Gorby et al.* [2006] showed that under controlled conditions, *S. oneidensis* MR-1 produced nanowires in response to electron acceptor limitation. In our experiments, oxygen-limited conditions rapidly developed at the start of the column 2 experiment and in the transition zone between the clean and iron (oxyhydr)oxide coated sand sections. However, SEM images (Figure 4b) show that individual *S. oneidensis* MR-1 cells had ready access to ferrihydrite as an alternative electron acceptor to O_2. Furthermore, not all observed cells displayed structures that could be classified as nanowires, suggesting that electron transport to ferrihydrite occurred via a range of mechanisms, e.g., direct transfer

through outer-membrane cytochromes or indirect transfer via the secretion of electron shuttles such as flavins [*von Canstein et al.*, 2008; *Reardon et al.*, 2010]. Hence, there is no overall evidence for an interconnected and conductive biofilm/nanowire network in column 2.

[25] In column 1, ferrihydrite concentrations were ~25 times lower than in column 2, and ferrihydrite was distributed in isolated patches over the surface of the sand grains (Figure S1a). Bacteria were initially associated with the natural sediment fraction (5% by volume) mixed in with the sand, and although some extracellular polymer substances were found, there was no evidence of a spatially continuous biofilm over the sand surfaces. This suggests that microbial Fe(III) reduction occurred in niches throughout the column fill, which may be more representative of natural sedimentary environments where the iron (oxyhydr)oxides will be heterogeneously distributed throughout the soil/sediment matrix alongside variable quantities of other mineral phases. We propose that the contrasting conditions in columns 1 and 2 demonstrate that electron donor amendments (e.g., acetate/lactate) can promote the bioreducing conditions necessary for immobilizing contaminants without the extensive biofilm or nanowire-network formation required by the biogeobattery hypothesis.

[26] The absence of a geobattery signature in this work appears to contrast with the results of *Ntarlagiannis et al.* [2007], who reported large SP signals in a static sand column, open to the atmosphere at the top, containing *S. oneidensis* MR-1 bacteria. SEM images showed that in their system the bacteria were connected to each other via the nanowire-type appendages investigated further by *Gorby et al.* [2006] and *El-Naggar et al.* [2010]. A +600 mV anomaly developed after 10 days between the reference electrode at the bottom of the column and an electrode at the top of the column. *Ntarlagiannis et al.* [2007] suggest a mechanism whereby electrons were transferred via the nanowire network from bacteria in the anaerobic part of the column to bacteria in the oxic top of the column with access to O_2 as the terminal electron acceptor. However, the Ag/AgCl SP electrodes used by *Ntarlagiannis et al.* [2007] were in direct contact with the pore waters, a configuration that can allow galvanic potentials to develop at the electrode-solution interface [*Williams et al.*, 2007; *Slater et al.*, 2008; *Zhang et al.*, 2010]. It is noteworthy that the positive polarity of the 600 mV signal reported by *Ntarlagiannis et al.* [2007] is consistent with a galvanic cell potential. Indeed, a geobattery mechanism would produce a negative anomaly between the reference and measurement electrodes, i.e., opposite to the change in redox potential [*Bigalke and Grabner*, 1997; *Castermant et al.*, 2008]. *Revil et al.* [2010] suggested repeating the experiments of *Ntarlagiannis et al.* [2007] using electrodes that are known to be insensitive to fluid chemistry (such as those used in our experiments; see section 2.5).

[27] The bacteria in the experiments of *Ntarlagiannis et al.* [2007] were cultured in a chemostat in oxygen-limited conditions and thus were deliberately primed for nanowire production. In contrast, we followed the general approach of *Hansel et al.* [2003], culturing the bacteria aerobically to late log phase growth before harvesting them for the column 2 experiment. This approach clearly resulted in microbial Fe(III) reduction but did not promote the development of a nanowire network. This result suggests that in future biogeobattery studies, bacteria must to be cultured very specifically to produce a nanowire network.

4.2. Conductive Biominerals

[28] Figures 3 and 4 show that during microbial Fe(III) reduction iron (oxyhyr)oxide mineral transformations also occurred in both of the column experiments. Formation of both goethite (Fe(III) oxyhydroxide) and magnetite (mixed Fe(II) and Fe(III) oxide) was observed in this study. Secondary Fe-mineral formation following ferrihydrite reduction is a complicated process dependent on Fe(II) and anion (Cl^-, SO_4^{2-}, HCO_3^-) concentrations, pH, and competing pathways of mineral dissolution/precipitation and solid-state mineral nucleation and growth [*Hansel et al.*, 2005]. Microbial Fe(III) reduction releases Fe(II) into solution, which is then adsorbed onto the ferrihydrite surface. This process leads to an electron transfer from the Fe(II) to the Fe(III) at the surface of the ferrihydrite, which causes the reduction of Fe(III) to form soluble Fe(II), while simultaneously the oxidized Fe(III) precipitates to form goethite. In this reaction the adsorbed Fe(II) acts as a catalyst (i.e., there is no net loss of Fe(II) from the system) for the reduction/dissolution and reprecipitation reaction mechanism of goethite crystallization from ferrihydrite [*Yee et al.*, 2006]. Sorbed Fe(II) can also drive the solid-state transformation of ferrihydrite to magnetite, although this process requires higher concentrations of Fe(II) or higher pH, or both, than the goethite formation process and occurs at a slower rate. Magnetite nucleation and growth can also occur at the expense of the initially formed goethite [*Hansel et al.*, 2003, 2005].

[29] The role of dissolved Fe(II) concentrations is clearly visible in columns 1 and 2, where magnetite formation is observed only at dissolved Fe(II) concentrations greater than ~0.5 m*M*. No magnetite formed in column 1 (Fe(II) ≤ 0.52 m*M*) and magnetite only formed at the top of column 2 after Fe(II) concentrations exceeded ~0.5 m*M* (see data for column 2 on day 7 in Figures 3 and 5). In the context of the biogeobattery model, the magnetite in column 2 provides an electrically conductive phase that could act as a conduit for electron flow between the different redox zones. However, the spatial relationship between redox zones and magnetite formation must be considered. Magnetite formed ~2.5 cm into the iron (oxyhydr)oxide coated sand section of the column, when Fe(II) concentrations exceeded 0.5 mM. This point of the column was firmly anoxic (Figure 5e), meaning that magnetite was not located across the oxic-anoxic redox boundary and therefore could not act as a geobattery conductor (Figure 1a). A scenario where such conduction might be possible is if magnetite were linked to the oxic zone via a conductive biofilm/nanowire network (Figure 1b) [*Revil et al.*, 2010]. As previously stated, such a network was not observed in column 2. Fluctuating fringes of a water table or groundwater plume may also expose a zone of magnetite biomineralization to a redox boundary. However, this exposure would be expected to result in oxidation of the nano-sized magnetite to a low-conductivity iron (oxyhydr)oxide, thereby removing the conductor. Furthermore, in sediments with natural microbial communities (e.g., column 1), the quantity of magnetite produced in situ may be very low, with competing mineral transformation pathways preferentially creating low-conductivity Fe-rich minerals such as green rusts, siderite, goethite, lepidocrocite, and vivianite [*Cornell and*

Schwertmann, 2003]. We therefore conclude that biominerals alone are unlikely to form effective conductors in a biogeobattery that forms across an oxic-anoxic boundary.

4.3. Return Current Pathway

[30] In the classical geobattery model depicted in Figure 1a, the chemical potential (redox) gradient in the groundwater is the thermodynamic driving force for current flow in the (ore body) conductor, which transports electrons from the area of low redox potential to the area of relatively high redox potential. *Revil et al.* [2010] argue that from the standpoint of potential field theory, the ore body is the current source. The electrical potential field is propagated outside the current source through the conductive pore fluid in the surrounding host rock. Transfer of charge between ionic species and the conductor occurs at the surface of the ore body, creating local charge imbalance in the solution [*Sato and Mooney*, 1960]. Charge balance in solution is maintained by the migration of ions in the electrical potential field toward/away from the cathode/anode. The pore fluid surrounding the ore body therefore acts as the return current pathway, completing the electrical circuit. The equivalent return current pathway for a biogeobattery would also be through the pore fluid surrounding the electronic conductor, i.e., the nanowire network (Figure 1b). An important question that still needs to be answered, however, is the effective scale over which a nanowire network transports charge. This question has implications for the optimal experimental design for biogeobattery investigations, including this study.

[31] *Ntarlagiannis et al.* [2007] suggested that a nanowire network could effectively transport charge over tens of centimeters. If the nanowire network acts as a single, electrically continuous unit, then the return current pathway will occur through an adjacent zone with no nanowire network, analogous to the host rock in the ore body geobattery model. A tank geometry similar to the experiments of *Naudet et al.* [2005] and *Castermant et al.* [2008] may therefore be the most appropriate design to detect the SP anomaly generated. In contrast, *Revil et al.* [2010] recently postulated that many discrete biogeobattery dipoles arranged in parallel along a redox boundary could combine to give the macroscopic dipole recorded by SP measurements. We infer that return current flow would therefore be localized to the pore fluid surrounding each dipole (Figure 1b). This scenario is arguably more likely at the field scale and would also be measurable in a column arrangement of the type we used, where laterally discontinuous nanowire formation at the redox boundary would allow return current flow through the pore fluid surrounding discrete biogeobattery dipoles (Figure 1b). Biogeobattery formation should therefore have been possible in our study if a nanowire network had formed.

4.4. Wider Implications

[32] Recent field investigations of biodegrading organic contaminant plumes [*Forté and Bentley*, 2010; *Slater et al.*, 2010] have shown that SP anomalies do not always occur where redox boundaries are present in the subsurface. This result highlights the importance of the redox gradient being collocated with a suitable conductor [*Revil et al.*, 2010]. Our study confirms this issue, and furthermore it is likely that the fine-grained conductive mineral phases produced from microbial Fe(III) reduction are susceptible to reoxidation when present at a nonstatic anoxic/oxic redox boundary. Contaminated sites can further complicate SP source mechanisms, as they often contain substantial amounts of buried metallic waste and structures, which can potentially act in the manner of a classic ore body geobattery or microbial fuel cell [*Doherty et al.*, 2010]. Field evidence of redox-associated SP anomalies shows that this technique can potentially provide powerful spatiotemporal information on redox conditions [*Naudet et al.*, 2004; *Doherty et al.*, 2010]. However, the continued lack of direct experimental verification of the source mechanisms, combined with the lack of SP anomalies at other field sites with redox gradients [*Forté and Bentley*, 2010; *Slater et al.*, 2010], means that SP cannot be used alone as a diagnostic tool. Complementary geophysical techniques such as spectral induced polarization are showing promise but also require further work to understand and model the underlying processes responsible for the geophysical responses [*Williams et al.*, 2009].

5. Conclusions

[33] We successfully developed contrasting redox conditions within flow-through column experiments with both indigenous and model Fe(III)-reducing microorganisms, creating one of the key components needed to form a biogeobattery. However, in our systems, no self-potential anomaly was detected. Although microbial Fe(III) reduction transformed ferrihydrite to goethite and, in column 2, subsequently developed the electrically more conductive magnetite, no evidence was found of a conductive biofilm or mineral network linking the different redox zones in the column. At present, direct experimental verification of the biogeobattery model remains elusive. The scale of electron transport and nanowire formation that is needed for a biogeobattery to form is still unconstrained and has important implications for the likely frequency of biogeobattery formation under field conditions. It is apparent from this study that biogeobattery generation is nontrivial and requires specific geochemical and microbiological conditions that, we conclude, will not occur at every contaminated site undergoing microbially mediated redox processes. Therefore we conclude that SP alone is unreliable as a noninvasive tool for monitoring changing redox conditions in the subsurface.

[34] **Acknowledgments.** This work was funded by Leverhulme Trust award F/00 122/AO and NERC grant NE/D014026/1; we acknowledge studentship support from the EPSRC to Diana Brookshaw. Thanks to Tony Windross and Rhys Moore for building the columns, Martin Fuller for SEM sample preparation, David Ashley for ion chromatography, and Dimitris Ntarlagiannis for help with electrode design. We also thank the editors and reviewers for their very useful comments on our manuscript.

References

Abdel Aal, G. Z., E. A. Atekwana, L. D. Slater, and E. A. Atekwana (2004), Effects of microbial processes on electrolytic and interfacial electrical properties of unconsolidated sediments, *Geophys. Res. Lett.*, *31*, L12505, doi:10.1029/2004GL020030.

Anderson, R. T., et al. (2003), Stimulating the in situ activity of *Geobacter* species to remove uranium from the groundwater of a uranium-contaminated aquifer, *Appl. Environ. Microbiol.*, *69*(10), 5884–5891, doi:10.1128/AEM.69.10.5884-5891.2003.

Arora, T., A. Revil, N. Linde, and J. Castermant (2007), Non-intrusive determination of the redox potential of contaminant plumes using the

self-potential method, *J. Contam. Hydrol.*, *92*, 274–292, doi:10.1016/j.jconhyd.2007.01.018.

Atekwana, E. A., and L. D. Slater (2009), Biogeophysics: A new frontier in Earth science research, *Rev. Geophys.*, *47*, RG4004, doi:10.1029/2009RG000285.

Begg, J. D. C., I. T. Burke, J. R. Lloyd, C. Boothman, S. Shaw, J. M. Charnock, and K. Morris (2011), Bioreduction behaviour of U(VI) sorbed to sediments, *Geomicrobiol. J.*, *28*, 160–171, doi:10.1080/01490451003761137.

Bigalke, J., and E. W. Grabner (1997), The Geobattery model: A contribution to large scale electrochemistry, *Electrochim. Acta*, *42*(23–24), 3443–3452, doi:10.1016/S0013-4686(97)00053-4.

Brooks, S. C., D. L. Taylor, and P. M. Jardine (1996), Reactive transport of EDTA-complexed cobalt in the presence of ferrihydrite, *Geochim. Cosmochim. Acta*, *60*, 1899–1908, doi:10.1016/0016-7037(96)00064-6.

Castermant, J., C. A. Mendonça, A. Revil, F. Trolard, G. Bourrié, and N. Linde (2008), Redox potential distribution inferred from self-potential measurements during the corrosion of a burden metallic body, *Geophys. Prospect.*, *56*, 269–282, doi:10.1111/j.1365-2478.2007.00675.x.

Catalano, J. G., J. P. McKinley, J. M. Zachara, S. M. Heald, S. C. Smith, and G. E. Brown Jr. (2006), Changes in uranium speciation through a depth sequence of contaminated Hanford sediments, *Environ. Sci. Technol.*, *40*(8), 2517–2524, doi:10.1021/es0520969.

Cornell, R. M., and U. Schwertmann (2003), *The Iron Oxides*, 2nd ed., 664 pp., Wiley-VCH, Weinheim, Germany, doi:10.1002/3527602097.

Doherty, R., B. Kulessa, A. S. Ferguson, M. J. Larkin, L. A. Kulakov, and R. M. Kalin (2010), A microbial fuel cell in contaminated ground delineated by electrical self-potential and normalized induced polarization data, *J. Geophys. Res.*, *115*, G00G08, doi:10.1029/2009JG001131.

El-Naggar, M. Y., G. Wanger, K. M. Leung, T. D. Yuzvinsky, G. Southam, J. Yang, W. M. Laud, K. H. Nealson, and Y. A. Gorby (2010), Electrical transport along bacterial nanowires from *Shewanella oneidensis* MR-1, *Proc. Natl. Acad. Sci. U. S. A.*, *107*, 18,127–18,131, doi:10.1073/pnas.1004880107.

Fennell, D. E., A. B. Carroll, J. M. Gossett, and S. H. Zinder (2001), Assessment of indigenous reductive dechlorinating potential at a TCE-contaminated site using microcosms, polymerase chain reaction analysis, and site data, *Environ. Sci. Technol.*, *35*(9), 1830–1839, doi:10.1021/es0016203.

Forté, S., and L. R. Bentley (2010), Mapping degrading organic contaminant plumes with spontaneous potential: Why does it not always work?, Abstract NS31B-1396 presented at 2010 Fall Meeting, AGU, San Francisco, Calif., 13–17 Dec.

Gorby, Y. A., et al. (2006), Electrically conductive bacterial nanowires produced by *Shewanella oneidensis* strain MR-1 and other microorganisms, *Proc. Natl. Acad. Sci. U. S. A.*, *103*, 11,358–11,363, doi:10.1073/pnas.0604517103.

Hansel, C. M., S. G. Benner, J. Neiss, A. Dohnalkova, R. K. Kukkadapu, and S. Fendorf (2003), Secondary mineralization pathways induced by dissimilatory iron reduction of ferrihydrite under advective flow, *Geochim. Cosmochim. Acta*, *67*, 2977–2992, doi:10.1016/S0016-7037(03)00276-X.

Hansel, C. M., S. G. Benner, and S. Fendorf (2005), Competing Fe(II)-induced mineralization pathways of ferrihydrite, *Environ. Sci. Technol.*, *39*, 7147–7153, doi:10.1021/es050666z.

Hunter, J. (2004), SCLS Phase 1—Conceptual Model of Contamination Below Ground at Sellafield, *Rep. NSTS 4920*, Nucl. Sci. and Technol. Serv., Br. Nucl. Fuels Ltd., London.

Jouniaux, L., A. Maineult, V. Naudet, M. Pessel, and P. Sailhac (2009), Review of self-potential methods in hydrogeophysics, *C. R. Geosci.*, *341*, 928–936, doi:10.1016/j.crte.2009.08.008.

Kelly, S. D., K. M. Kemner, J. Carley, C. Criddle, P. M. Jardine, T. L. Marsh, D. Phillips, D. Watson, and W.-M. Wu (2008), Speciation of uranium in sediments before and after in situ biostimulation, *Environ. Sci. Technol.*, *42*, 1558–1564, doi:10.1021/es071764i.

Law, G. T. W., A. Geissler, C. Boothman, I. T. Burke, F. R. Livens, J. R. Lloyd, and K. Morris (2010a), Role of nitrate in conditioning aquifer sediments for technetium bioreduction, *Environ. Sci. Technol.*, *44*, 150–155, doi:10.1021/es9010866.

Law, G. T. W., et al. (2010b), Geomicrobiological redox cycling of the transuranic element neptunium, *Environ. Sci. Technol.*, *44*, 8924–8929, doi:10.1021/es101911v.

Lear, G., J. M. McBeth, C. Boothman, B. Ellis, R. Lawson, K. Morris, N. D. Bryan, I. T. Burke, F. R. Livens, and J. R. Lloyd (2010), Probing the biogeochemical behaviour of technetium using a novel nuclear imaging approach, *Environ. Sci. Technol.*, *44*, 156–162, doi:10.1021/es802885r.

Lovley, D. R., and E. J. P. Phillips (1987), Rapid assay for microbially reducible ferric iron in aquatic sediments, *Appl. Environ. Microbiol.*, *53*, 1536–1540.

Maineult, A., Y. Bernabé, and P. Ackerer (2006), Detection of advected, reacting redox fronts from self-potential measurements, *J. Contam. Hydrol.*, *86*, 32–52, doi:10.1016/j.jconhyd.2006.02.007.

Minsley, B. J., J. Sogade, and F. D. Morgan (2007), Three-dimensional self potential inversion for subsurface DNAPL contaminant detection at the Savannah River Site, South Carolina, *Water Resour. Res.*, *43*, W04429, doi:10.1029/2005WR003996.

Naudet, V., and A. Revil (2005), A sandbox experiment to investigate bacteria-mediated redox processes on self-potential signals, *Geophys. Res. Lett.*, *32*, L11405, doi:10.1029/2005GL022735.

Naudet, V., A. Revil, E. Rizzo, J. Y. Bottero, and P. Bégassat (2004), Ground water redox conditions and conductivity in a contaminant plume from geoelectrical investigations, *Hydrol. Earth Syst. Sci.*, *8*(1), 8–22, doi:10.5194/hess-8-8-2004.

Ntarlagiannis, D., K. H. Williams, L. Slater, and S. Hubbard (2005), The low frequency electrical response to microbially induced sulfide precipitation, *J. Geophys. Res.*, *110*, G02009, doi:10.1029/2005JG000024.

Ntarlagiannis, D., E. A. Atekwana, E. A. Hill, and Y. Gorby (2007), Microbial nanowires: Is the subsurface "hardwired"? *Geophys. Res. Lett.*, *34*, L17305, doi:10.1029/2007GL030426.

Petiau, G. (2000), Second generation of lead-lead chloride electrodes for geophysical applications, *Pure Appl. Geophys.*, *157*, 357–382, doi:10.1007/s000240050004.

Reardon, C. L., et al. (2010), Role of outer-membrane cytochromes MtrC and OmcA in the biomineralization of ferrihydrite by *Shewanella oneidensis* MR-1, *Geobiology*, *8*, 56–68, doi:10.1111/j.1472-4669.2009.00226.x.

Reguera, G., K. D. McCarthy, T. Mehta, J. S. Nicoll, M. T. Tuominen, and D. R. Lovley (2005), Extracellular electron transfer via microbial nanowires, *Nature*, *435*, 1098–1101, doi:10.1038/nature03661.

Reguera, G., K. P. Nevin, J. S. Nicoll, S. F. Covalla, T. L. Woodard, and D. R. Lovley (2006), Biofilm and nanowire production leads to increased current in *Geobacter sulfurreducens* fuel cells, *Appl. Environ. Microbiol.*, *72*, 7345–7348, doi:10.1128/AEM.01444-06.

Revil, A., C. A. Mendonça, E. A. Atekwana, B. Kulessa, S. S. Hubbard, and K. J. Bohlen (2010), Understanding biogeobatteries: Where geophysics meets microbiology, *J. Geophys. Res.*, *115*, G00G02, doi:10.1029/2009JG001065.

Reynolds, J. M. (1997), *An Introduction to Applied and Environmental Geophysics*, 806 pp., John Wiley, Chichester, U.K.

Sato, M., and H. M. Mooney (1960), The electrochemical mechanism of sulfide self-potentials, *Geophysics*, *25*, 226–249, doi:10.1190/1.1438689.

Slater, L., D. Ntarlagiannis, N. Yee, M. O'Brien, C. Zhang, and K. H. Williams (2008), Electrodic voltages in the presence of dissolved sulfide: Implications for monitoring natural microbial activity, *Geophysics*, *73*(2), F65–F70, doi:10.1190/1.2828977.

Slater, L. D., et al. (2010), Investigation of biogeophysical signatures at a mature crude-oil contaminated site, Bemidji, Minnesota, Abstract NS31B–1397 presented at 2010 Fall Meeting, AGU, San Francisco, Calif., 13–17 Dec.

Stookey, L. L. (1970), Ferrozine—A new spectrophotometric reagent for iron, *Anal. Chem.*, *42*, 779–781, doi:10.1021/ac60289a016.

Stumm, W., and J. J. Morgan (1981), *Aquatic Chemistry: An Introduction Emphasizing Chemical Equilibria in Natural Waters*, 2nd ed., 780 pp., John Wiley, New York.

Vandevivere, P., and P. Baveye (1992), Sampling method for the observation of microorganisms in unconsolidated porous media via scanning electron microscopy, *Soil Sci.*, *153*, 482–485, doi:10.1097/00010694-199206000-00007.

von Canstein, H., J. Ogawa, S. Shimizu, and J. R. Lloyd (2008), Secretion of flavins by *Shewanella* species and their role in extracellular electron transfer, *Appl. Environ. Microbiol.*, *74*, 615–623, doi:10.1128/AEM.01387-07.

Wilkins, M. J., F. R. Livens, D. J. Vaughan, I. Beadle, and J. R. Lloyd (2007), The influence of microbial redox cycling on radionuclide mobility in the subsurface at a low-level radioactive waste storage site, *Geobiology*, *5*, 293–301, doi:10.1111/j.1472-4669.2007.00101.x.

Williams, K. H., S. S. Hubbard, and J. F. Banfield (2007), Galvanic interpretation of self-potential signals associated with microbial sulfate-reduction, *J. Geophys. Res.*, *112*, G03019, doi:10.1029/2007JG000440.

Williams, K. H., A. Kemna, M. J. Wilkins, J. Druhan, E. Arntzen, L. N'Guessan, P. Long, S. S. Hubbard, and J. Banfield (2009), Geophysical monitoring of microbial activity during stimulated subsurface bioremediation, *Environ. Sci. Technol.*, *43*(17), 6717–6723, doi:10.1021/es900855j.

Yee, N., S. Shaw, L. G. Benning, and T. H. Nguyen (2006), The rate of ferrihydrite transformation to goethite via the Fe(II) pathway, *Am. Mineral.*, *91*, 92–96, doi:10.2138/am.2006.1860.

Zhang, C., D. Ntarlagiannis, L. Slater, and R. Doherty (2010), Monitoring microbial sulfate reduction in porous media using multipurpose electrodes, *J. Geophys. Res.*, *115*, G00G09, doi:10.1029/2009JG001157.

D. Brookshaw, J. R. Lloyd, and K. Morris, School of Earth, Atmospheric, and Environmental Sciences, University of Manchester, Oxford Road, Manchester M13 9PL, UK.

C. G. Hubbard, S. Shaw, and L. J. West, Earth Surface Science Institute, School of Earth and Environment, University of Leeds, Woodhouse Lane, Leeds LS2 9JT, UK. (L.J.West@leeds.ac.uk)

B. Kulessa, School of the Environment and Society, University of Swansea, Singleton Park, Swansea SA2 8PP, UK.